Medical and Pharmaceutical Journal

Volume 3 Issue 4

Med. Pharm. J. Original article

Computational Method of Molecular Dynamics Simulation Identifies Insulin Receptor Binding Site 2 as the Primary Site for Insulin Binding

Saousen R **Diaf** [1*], Ra'ed **Khashan**[2], Preston **Moore**[3]

[1] Department of Pharmaceutical Sciences, Philadelphia College of Pharmacy, Saint Joseph University, 19131, Philadelphia, PA, United States

[2] Department of Division of Pharmaceutical Sciences, Long Island University, United States

[3] Professor and Chair, Department of Chemistry Director, West Center for Computational Chemistry and Drug Design, Saint Joseph University, Philadelphia, Pennsylvania 19104, United States

***Corresponding Author**: Saousen R **Diaf**
Email: sd20629070@sju.edu

DOI: 10.55940/medphar202488
Submitted: 19-Aug -2023
Accepted: 15- Dec -2024
Published: 30-Jan-2025

ABSTRACT

Background: Insulin receptor (IR) is a homo-dimeric, extensively glycosylated, disulfide-linked, transmembrane tyrosine kinase receptor. IR has two distinctive insulin binding sites, suggesting a process of sequential insulin interactions characterized by negative cooperativity. The crystal structure of the dimeric IR ectodomain [PDB: 4ZXB] provides structural bases for this theory.

Objective: Identifies Insulin Receptor Binding Site 2 as the Primary Site for Insulin Binding

Methods: Molecular dynamics (MD) simulation is performed to study the initial association of insulin with its receptor, leading to full interaction. MD simulation serves as a bridge between theory and experiments, enabling simulations not feasible in the lab. The study utilized the crystal structures of the insulin receptor (PDB: 4ZXB) and insulin molecule (PDB: 1MSO). GROMACS, a tool developed by Groningen University, is used for the molecular dynamics application. Prior to simulation, the receptor was prepared by restoring missing residues and removing those used for crystallization. GROMACS, compatible with several other tools, supported the MD simulations.

Results: During 230 ns of all-atom, explicit-water MD simulations (0.75 million atoms), insulin and ECD-IR exhibited significant asymmetric interdomain and intersubunit conformational fluctuations without altering quaternary structures. Variations in insulin orientation and location, alongside subtle changes in residual contact of ECD-IR, coincided with these fluctuations. The insulin-IR site 2 interaction also induced interdomain conformational changes between the monomers at the subdomains L1-FnIII-2' (L1'-FnIII-2), with initial separation studied through RMSD calculations, showing a value of 3.3Å starting at 60 ns of simulation. This protein unfolding suggests a step towards major conformational changes in ECD-IR.

Conclusion: Molecular dynamics simulations provided insights into the sequential binding process and structural dynamics of the insulin-IR complex.

KEYWORDS: Molecular dynamics; Insulin; Insulin receptor; Protein structure; insulin receptor site-2; conformational flexibility

INTRODUCTION

Diabetes is a serious, long-term ailment that impacts the lives and well-being of people worldwide. It is a metabolic condition caused by the loss of pancreatic β cells through various processes, resulting in persistent hyperglycemia. While β cell loss occurs in all types of diabetes, it is particularly significant in type 1 diabetes mellitus (T1DM) and type 2 diabetes (T2D). Diabetes ranks among the top ten causes of death in adults, accounting for an estimated four million deaths globally in 2017, with global diabetes health spending predicted to reach USD 727 billion. In 2019, over 9.3 percent of the global adult population had diabetes; this figure is expected to grow to nearly 11 percent by 2045 [1].

The dysfunction of the insulin receptor has been linked not only to diabetes mellitus (T2D) but also to other severe pathologies, including cancer and Alzheimer's disease [37]. While Type 1 diabetes, or "insulin-dependent" diabetes, can be treated with exogenous insulin, Type 2 diabetes treatment depends on a molecular-level understanding of the insulin receptor, insulin, and the pathways by which insulin interacts with its receptor to trigger glucose uptake from the blood [2]. Several insulin analogs on the market are designed to mimic secreted insulin. These modifications typically occur at the C-terminal of the B-chain of insulin (B28-B31), but none of these residues are involved in insulin receptor interaction; they mainly influence insulin delivery and pharmacokinetic profiles. This raises the question: if we understood how insulin binds to its receptor, could we improve these analogs [3, 38].

To enhance the quality of life for diabetics, better structure-based designs of insulin mimetics, formulations, and nanotechnology-based delivery systems are required. These efforts necessitate a thorough structural understanding of insulin and its receptor, how the insulin receptor relays signals, the conformational dynamics and allostery that facilitate insulin-receptor interaction, and the development of testable hypotheses for therapeutic designs targeting insulin and its receptor.

Advancements in technologies such as X-ray crystallography and high-resolution cryo-electron microscopy have enabled 3-D atomic-level imaging of insulin, the insulin receptor, and their complex, revealing a wealth of information. Despite these advances, much remains to be learned about the insulin receptor, insulin signaling, and how to use this knowledge to improve the treatment of type 2 diabetes and other insulin-resistant states.

Insulin, produced in the β-cells of the islets of Langerhans as proinsulin, includes a C-peptide connecting the A- and B-chains [40]. Once proinsulin moves from the endoplasmic reticulum to the Golgi apparatus of the β-cell, the C-peptide is cleaved by specific endopeptidases, resulting in the mature form of insulin [37]. Insulin is a small peptide hormone with 51 residues that regulates blood glucose levels. It is a compact globular protein, 5.8 kDa in size, composed of two interlinked polypeptide chains: a 30-residue B-chain and a 21-residue A-chain [39, 4]. Insulin engagement is mediated by two binding surfaces: the hormone's classical

receptor-binding surface, which overlaps with its dimer-forming surface, and a second receptor-binding surface, which overlaps with the hormone's hexamer-forming surface. Full functionality of insulin requires the generation of additional surfaces through conformational changes that expose the hormone's core [4-7].

The insulin receptor (IR) contains 1,370 amino acids and has a molecular weight of 300-350 kDa. It consists of two identical α subunits and two identical β subunits, forming an Λ-shaped, two-fold symmetric structure [4, 5, 8]. The mature (αβ)2 receptor is formed after glycosylation, dimerization, and proteolytic processing of receptor precursors. The IR is a multi-domain structure composed of a leucine-rich repeat domain (L1), a cysteine-rich region (CR), a second leucine-rich repeat domain (L2), and three predicted fibronectin type III domains (FnIII-1, FnIII-2, and FnIII-3). Additionally, there is a domain of 120 residues (ID) located within FnIII-2, containing the α-CT helix. The apo ectodomain membrane entry points of domains FnIII-3 and FnIII-3' are separated by approximately 120 Å, connecting through the plasma membrane via a single helix transmembrane domain, followed by an intracellular juxta-membrane segment, a tyrosine kinase domain, and a C-terminal tail to the cytoplasmic kinase domain [Fig.2A]. This separation holds the intracellular tyrosine kinase domains apart, preventing their transphosphorylation. Single-particle electron microscopy of the full-length IR in lipid nanodiscs has verified that this apo conformation is maintained in the membrane context [9, 10]. Insulin binding is proposed to alter the Λ-shaped conformation into a T-like shape, bringing the FnIII-3 modules closer together, enabling transmembrane signaling and the transphosphorylation of the intracellular tyrosine kinase domains [9, 11].

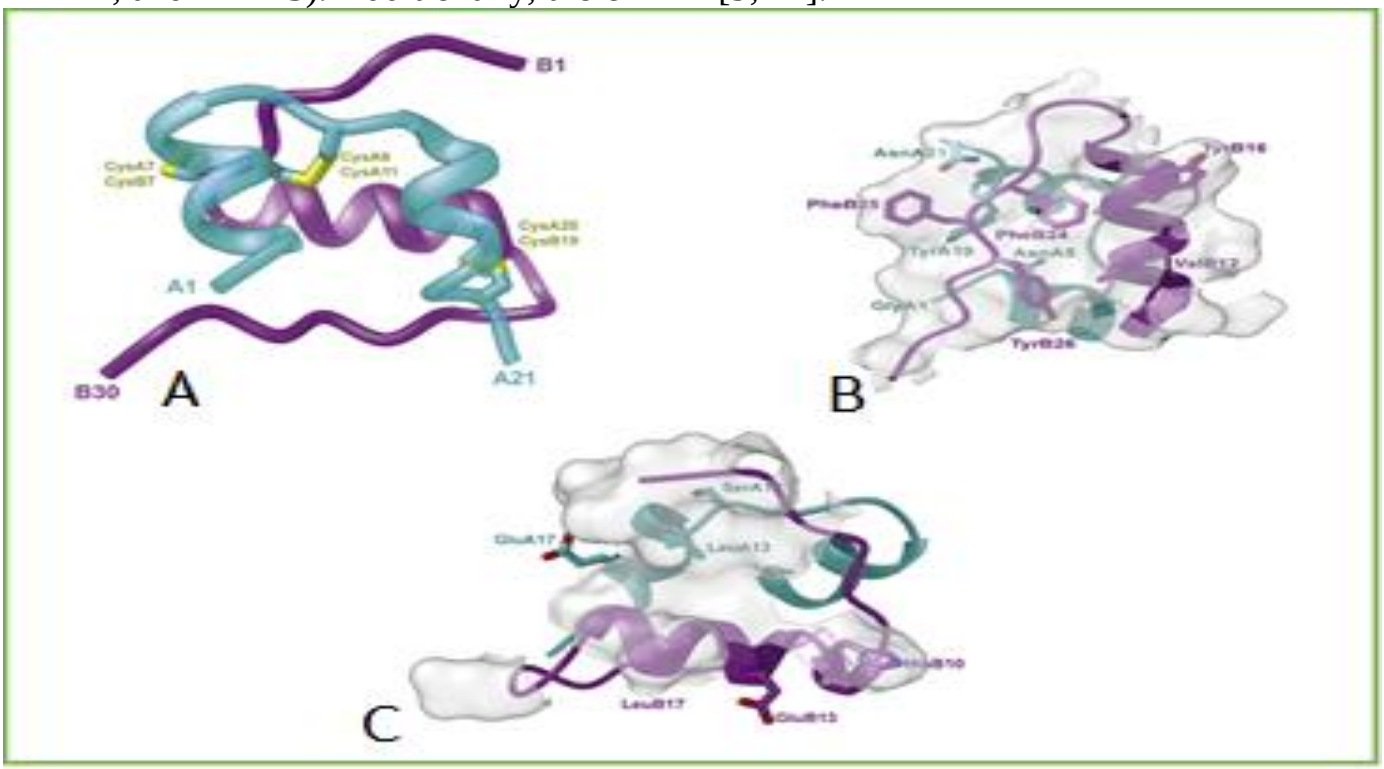

Figure 1: Structure of insulin (A) Structure of the insulin monomer showing chains A (cyan) and B

(magenta) together with two inter-chain disulfide bonds and one intra-chain disulfide bond. (B) The "classical" set of receptor-binding residues of insulin (stick representation) overlap with the dimer-forming surface(C) The receptor-binding residues of insulin (stick representation); these overlap insulin's hexamer-forming

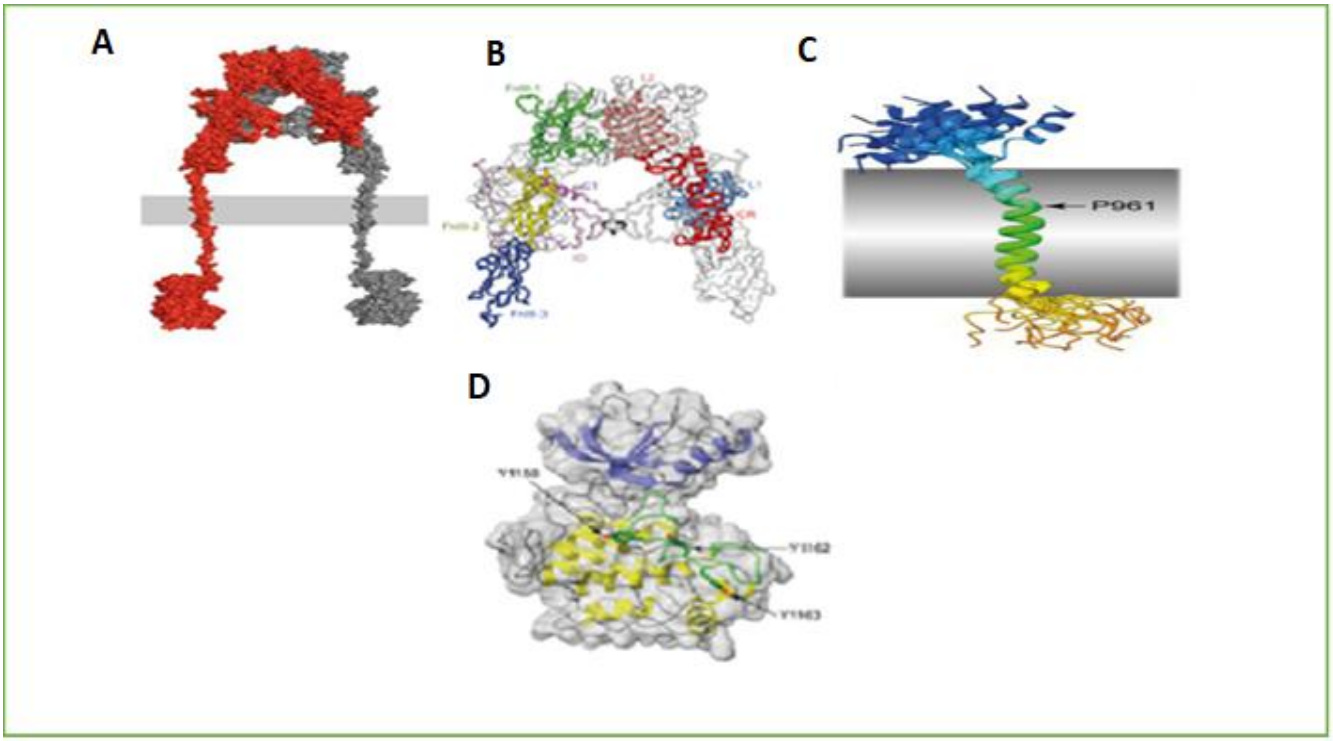

Figure 2: Structure of insulin receptor different domains (A) Structural model of the full-length human $(\alpha\beta)_2$ IR assembled from (ECD,TKD,TMD) (B) αβ monomer of ECD-IR in an Inverted V-shaped arrangement of the domains (C) Insulin receptor TM domain (D) Bi-lobal structure of the TKD-IR (N-terminal lobe in blue, C-terminal lobe in yellow and the activation loop in green 3)

The insulin receptor (IR) is an intertwined domain-swapped homodimer. Experimental studies on IR systems have elucidated that the interaction between the ligand (insulin) and receptor occurs via two distinct surfaces known as "site 1" and "site 2" [5, 12].

Site 1 comprises elements such as the leucine-rich repeat domain (L1), the α-CT helix, and the FnIII-1 domain, forming two interfaces with insulin: site 1a and site 1b (see Fig. 3). At the site 1a interface, insulin interacts with the L1 domain and α-CT helix from two different IR protomers. At the site 1b interface, the same insulin molecule interacts with a loop of the membrane-distal FnIII-1 domain from the IR protomer that donated the α-CT helix [12].

On the other hand, Site 2 is located on the backside of a major β sheet of the FnIII-1 domain from the IR protomer that contributed the α-CT helix of site 1 (see Fig. 3) [12- 14]. These detailed structural insights into the interactions at site 1 and site 2 provide a deeper understanding of how insulin engages with the IR and triggers downstream signaling events critical for glucose uptake and metabolic regulation.

The intrinsic tyrosine kinase activity and cellular signal transduction of the insulin receptor (IR) upon ligand interaction are

driven by major conformational changes and allosteric conformational transduction within the receptor [15, 16]. While atomically resolved structures of truncated IR constructs have illuminated conformational changes in individual domains, understanding the structural relationships and connectivity among these domains remains incomplete, hindering a full comprehension of the signaling molecular mechanism [4, 17].

The central aim of this project is to develop an understanding of the pathway of insulin and IR interaction, specifically by exploring the molecular mechanism at their initial point of contact. In this study, computational methods employing all-atom molecular dynamics (MD) simulations were conducted on structures (PDB ID: 1MSO & 4ZXB) in explicit solvent. MD simulation is a highly promising tool for elucidating the conformational flexibility of receptor structures and their ligand-binding mechanisms [18, 19].

Overall, the results from the MD simulations suggest a molecular model where insulin initially interacts with one of the exposed sites on the insulin receptor (site 2). This interaction induces residual rearrangements and the formation of salt bridges at the apex of the extracellular domain (ECD), which are crucial for controlling the number of insulin molecules interacting at site 1, a phenomenon known as negative cooperativity [20]. Furthermore, insulin site 2-IR interactions lead to alterations in the cross-talk between the L1 and FnIII-2 domains, facilitating specific T-shape domain-domain interactions [4].

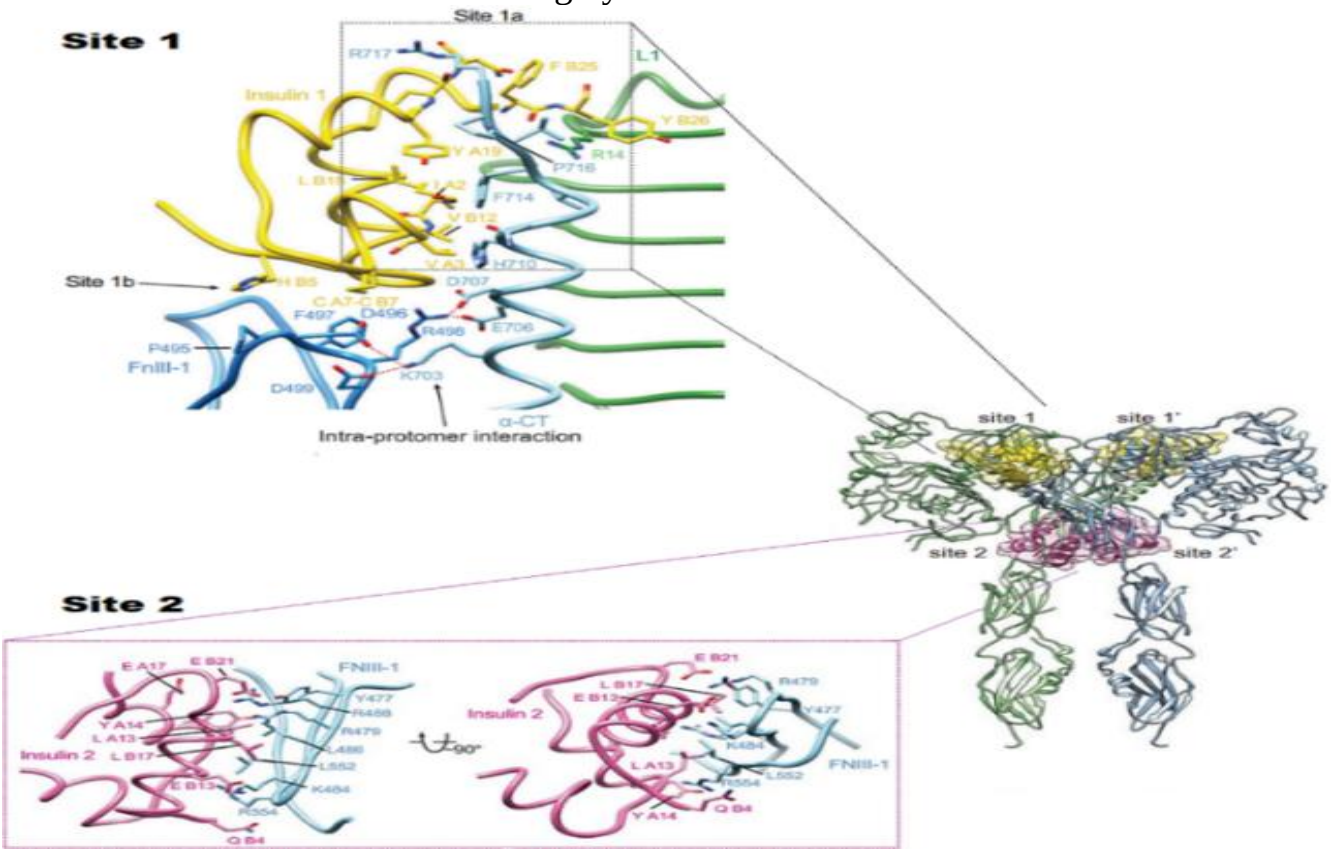

Figure 3: IR site1(1') and site2(2') locations. Ribbon representation of the IR dimer with four insulin bound complex (right panel). Close-up view of insulin-binding site1. (upper left panel). Close-up view of insulin-binding site2. (lower left panel).

MATERIAL AND METHODS

Molecular dynamic simulations

The crystal structures of the insulin receptor (PDB: 4ZXB) [5] and insulin molecule (PDB: 1MSO) [6] served as the base structures for molecular dynamics simulations. The co-crystallized IgG Fab fragments were removed [21], followed by the restoration of intentionally removed or accidentally missing amino acid residues from both structures. The ectodomain had several missing residues, which were removed to aid in modeling the structure of ECD-IR using X-ray crystallography. Specifically, the removed residues were located at the furin cleavage site (residues 720-723) and at the disordered and highly glycosylated N-terminal region of the IRβ subunit (residues 724-756) (Table 1). All residue modeling procedures were performed using MODELLER [42, 43], a computer program for homology modeling to generate tertiary and quaternary structures. The output structure from MODELLER was refined using UCSF CHIMERA [44], which serves as the graphical interface for MODELLER.

The insulin molecule was initially placed at an arbitrary position in the aqueous phase, at least 20 Å away from the surface of the receptor's binding pockets. For all simulations, calculations were conducted using the GROMACS 2023.3 package with the OPLS force field [16]. The box dimensions ensured that no protein atom was closer than 1.5 Å to the box wall, employing periodic boundary conditions and solvating with simple point charge (SPC/E) water molecules. Sodium counter ions were added for electro-neutrality. Energy minimization utilized the steepest descent method, followed by V-rescale temperature coupling and Parrinello-Rahman pressure coupling to maintain stability (300 K, 1 bar), with coupling constants set to 0.1 and 2.0 ps for temperature and pressure, respectively. The partial mesh Ewald (PME) algorithm was employed for electrostatic and van der Waals interactions, with a cutoff distance (rvdw) of 1.0 nm for short-range van der Waals interactions, while Coulomb (r coulomb) and neighbor list (rlist) cutoffs were set to 1.0 nm. All bond lengths were constrained using the LINCS algorithm, and the time step was set to 0.002 ps. The system was equilibrated for 100 ps in NVT and NPT ensembles, respectively, before conducting a 200-ns molecular dynamics simulation. Trajectories were recorded every 10 ps. Analysis included root-mean-square deviation (RMSD) from the initial structure, root-mean-square fluctuations (RMSF), and hydrogen bond formation. Modules such as g_rmsd, g_gyrate, and g_rmsf were employed to calculate the root mean square fluctuations and radius of gyration, considering all atoms of the protein.

RESULTS

Simulated Pose Matches experimental insulin- IR site 2 binding

During the simulation of insulin behavior, two simultaneous events are observed. The first event is the reorientation and directional change of the insulin molecule, causing its hexamer-forming surface to face and expose itself to the insulin receptor surface. Concurrently, the insulin molecule moves toward the insulin receptor. These variations in

orientation and location reach their maximum around 60 ns of simulation time (Fig. 6, 9).

The initial structure of the insulin molecule used in our simulations was obtained from the Protein Data Bank, specifically the T-state form of insulin (PDB: 1MSO). At 5 ns of simulation time, a change in insulin conformation is noted, with insulin temporarily adopting the R-state form (PDB: 1ZNI) [24]. The difference between these two states occurs in the N-terminal of chain B, within residues F1-G8. In the T-state form, the N-terminal of chain B is configured as an extended loop, whereas in the R-state form, the loop is coiled (Fig. 4A, B)

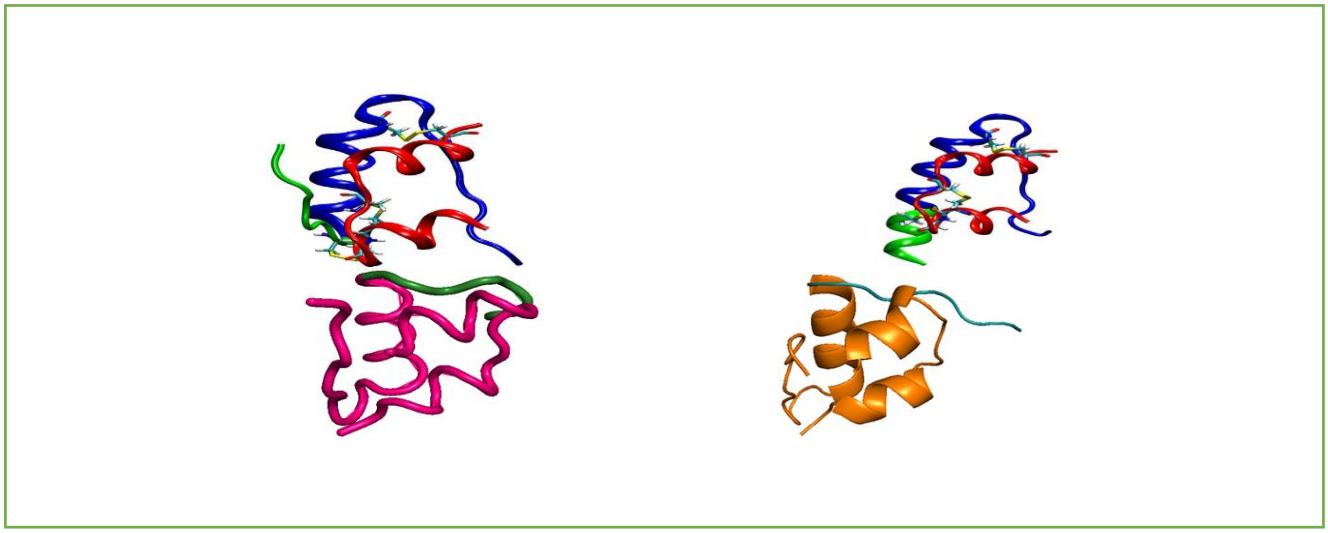

Figure 4: T- and R-insulin. (A and B) are shown: A-chain, red and B-chain, blue. (C and D) Insulin at 6ns simulation and the starting structure. The first eight residues of the B-chain, B1-B8, are in green cartoon

Molecular Dynamics

Root mean square deviations (RMSD)

The main chain root mean square deviations (RMSD) were calculated for the trajectories of the insulin and insulin receptor. The RMSD was calculated using the trajectory file for the backbone after least squares fitting to the C-alpha atoms using the "g_rms" tool. It is evident that the insulin receptor (IR) structure maintained almost the same starting conformation throughout the 230 ns of simulation time, resulting in a backbone maximum RMSD value of about 1 nm (Figure 5A). Meanwhile, the insulin reached a highest deviation of 1.5 nm. The initial maximum deviation in RMSD for insulin from the starting structure was observed around the first 60 ns, with another significant deviation at 200 ns (Fig. 5B). The RMSD of both structures, insulin and the insulin receptor, remained constant throughout the rest of the time period.

To determine the dynamic behavior of residues, RMSF values of the insulin and insulin receptor structures were calculated. The RMSF value of insulin receptor residues fluctuated within a range of 0.5–8 nm over the entire simulation period, with the majority of residues fluctuating between 0.5 and 4 nm. The maximum flexibility of 8 nm is

exhibited by residues located in FnIII-1, specifically at the αCT subdomain closer to site 1 of insulin interaction (Fig. 6A).
Additionally, the root mean square fluctuations (RMSF) of insulin were calculated over the trajectories and averaged over each residue during the molecular dynamics simulations. These fluctuations ranged from 0.5 to 2 nm. The graph indicates that the largest fluctuations of amino acids occurred in the C-terminal regions of chain A and chain B (Fig. 6B), while amino acids outside these regions showed lower fluctuations.

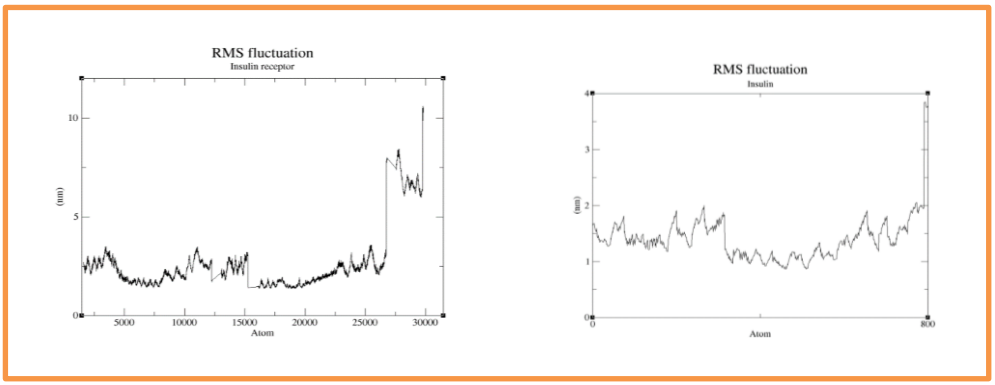

Figure 5: Backbone RMSDs at 300K are shown for: (A) Insulin receptor (B) Insulin molecule (C) Insulin Vs Insulin receptor (D)

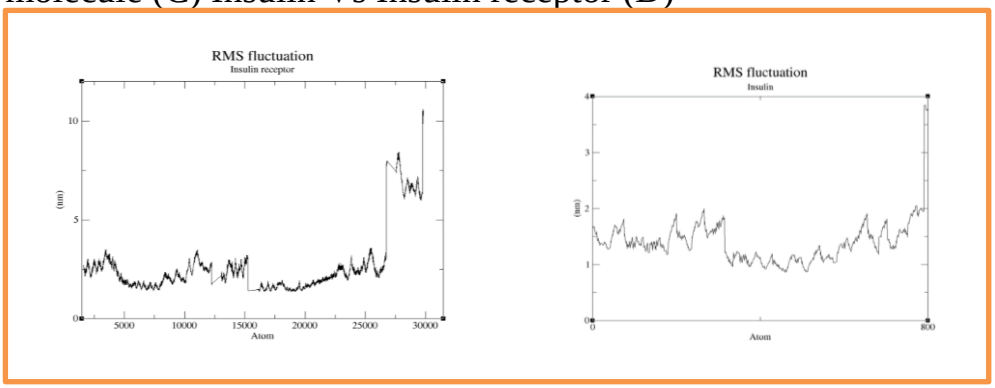

Figure 6: Backbone RMSFs at 300K are shown for: (A) Insulin receptor (B) Insulin molecule

Radius of Gyration (Rg)

The radius of gyration (Rg) is used to determine the compaction level in the structures of insulin and the insulin receptor. A plot of Rg for the Cα atoms of insulin and the insulin receptor over 200 ns of simulation time at 300 K was obtained using GROMACS tools. The curve for the insulin receptor reveals a steady Rg value throughout the entire simulation period (Fig. 7B).
On the other hand, the Rg profile for insulin shows an increased Rg value at the beginning of the simulation until approximately 60 ns. After this point, the system (insulin and insulin receptor) equilibrates and remains steady for the rest of the 200 ns simulation period (Fig. 7B & Fig. 7C).

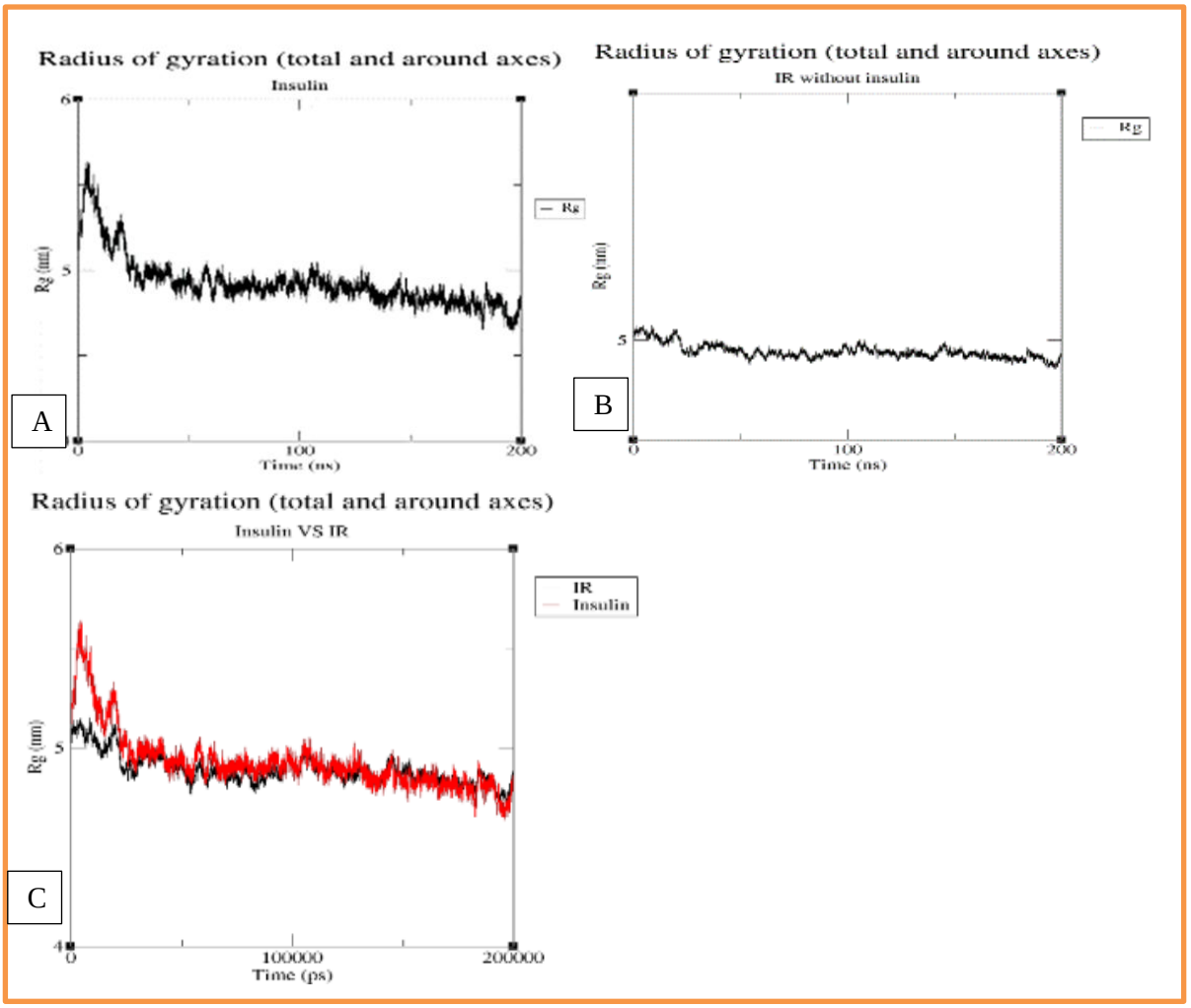

Figure 7: Radius of Gyration Rg of Ca atoms of: (A) insulin and (B) insulin receptor (C) Insulin vs IR

Insulin-insulin receptor initial contact

In all the simulations, insulin behaves in similar ways in its interaction with the insulin receptor. At the beginning of the simulation, insulin temporarily adopts the configuration of the R-state before returning to the T-state prior to any direct association with the receptor. In our study, except for a non-persistent interaction at 9 ns where AsnA18 forms an intermittent hydrogen bond with site 2 residue Lys544, no interaction was observed between insulin and the insulin receptor until 15 ns of simulation time.

Our simulations suggest that two main changes occur along the pathway leading to the interaction of insulin with site 2. The first change is the reorientation of insulin without significant conformational changes within the molecule itself. This reorientation brings the hexamerizing surface of insulin into closer contact with the receptor surface. The reorientation of insulin occurs simultaneously with its movement towards the receptor surface. This likely leads to the dehydration of both the ligand and the extracellular surface of the insulin receptor, bringing the ligand into close proximity with the β-sheet of site 2 on the receptor (Fig. 8).

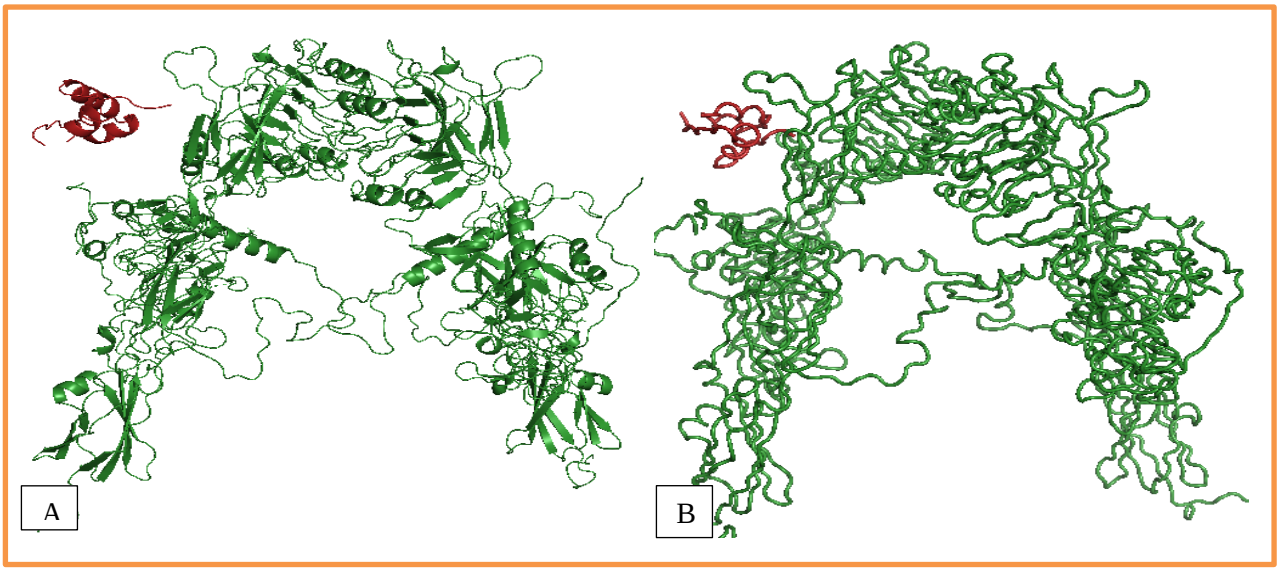

Figure 8**:** Insulin reorientation and movement towards IR. A) Starting structure of simulation, Insulin (red), IR (green). B) Simulated structure at 15ns with new insulin site (red)

A fast interaction takes place at 15 ns of the simulation, where insulin shows its first association with the insulin receptor (IR). Insulin's dynamic behavior towards the insulin receptor leads to the formation of the first interaction through a single hydrogen bond between EA17, an insulin residue at chain A, and K544, an IR residue located at FnIII-1 site 2. As the simulation proceeds, more residues from insulin become involved with the insulin receptor, resulting in stronger interactions with site 2, as demonstrated in Figure 9, showing simulations at 15, 20, 60, and 112 ns.

At 20 ns of simulation, three hydrogen bonds are formed: one between EA17 and K544, and two others between EB42 and R479 and EB42 with R488. The 60 ns simulation shows the formation of two hydrogen bonds: one between EB42 and R479, and another between RB43 and Q546. The simulation at 135 ns shows hydrogen bonds at site 2 formed between EB42 and R554, and YB37 with K484. Additionally, the insulin residue FB22 is observed to interact with Glu316 of the L2 subdomain of the alternate monomer with a single hydrogen bond, though this interaction is intermittent and often breaks during the simulation.

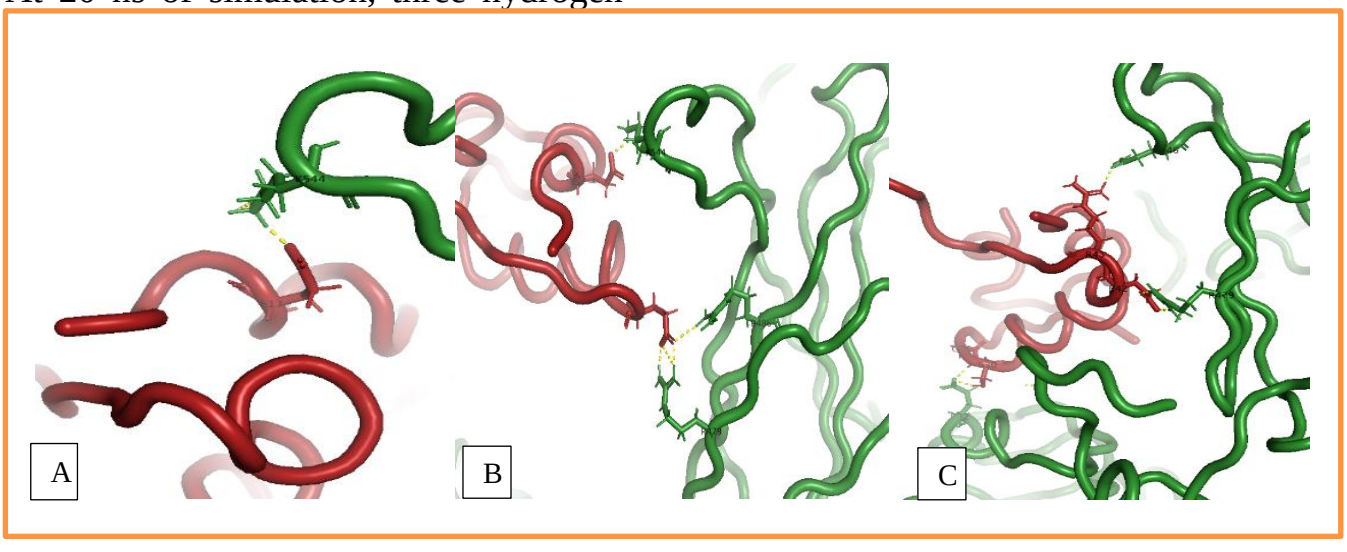

Figure 9**:** insulin-IR-ECD interaction at different simulation time. (A) interaction at 15ns, shows a single hydrogen bond between E17 and K544. (B) interactions at 20ns, shows 3 hydrogen bonds, one between E17 and K544, the other 2 between E42 and R479/R488. (C) interactions at 60ns 2 hydrogen bonds are formed E42 with R479 and R43with Q546.

Starting at 101 ns of the simulation, insulin becomes more involved with the insulin receptor (IR), while maintaining the site 2 interaction with FnIII-1. Interactions spread to involve subdomains L1 and CR, with hydrogen bonding formed between SA12 and E316, SB30 and E22, and HB31 and R19 (Fig. 10A). At 125 ns of the simulation, additional interactions between insulin and IR at the L1 and CR subdomains occur: SA12 interacts with E316 using three hydrogen bonds and interacts with R791 using two hydrogen bonds, QA5 with N268, IA10 with C274, and SA9 with K265 (Fig. 10B). However, as the simulation continues, insulin starts to lose interactions with site 2 of the ECD-IR. By 200 ns, the interactions are between EA17 and K544, EA42 and R479, and FB22 and E316 (Fig. 11), along with interactions involving QA5 and SB30. The reduction of interactions continues even after 230 ns, involving SA11, SB30, and HB31.

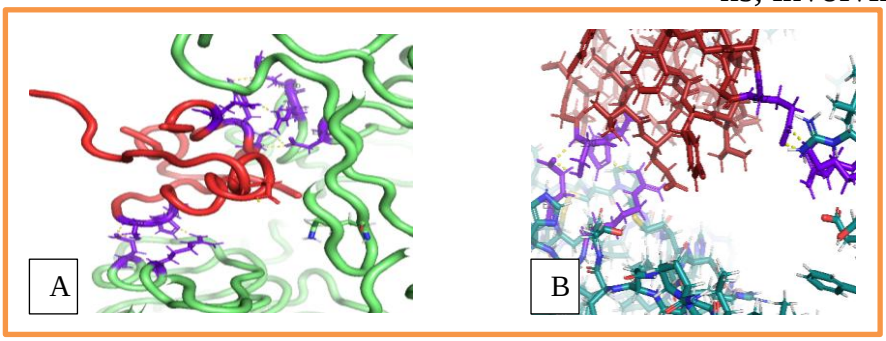

Figure10: Insulin-ECD-IR complex. (A) insulin-ECD-IR complex at 101ns with different interactions between insulin and IR. (B) insulin-ECD-IR complex at 125ns

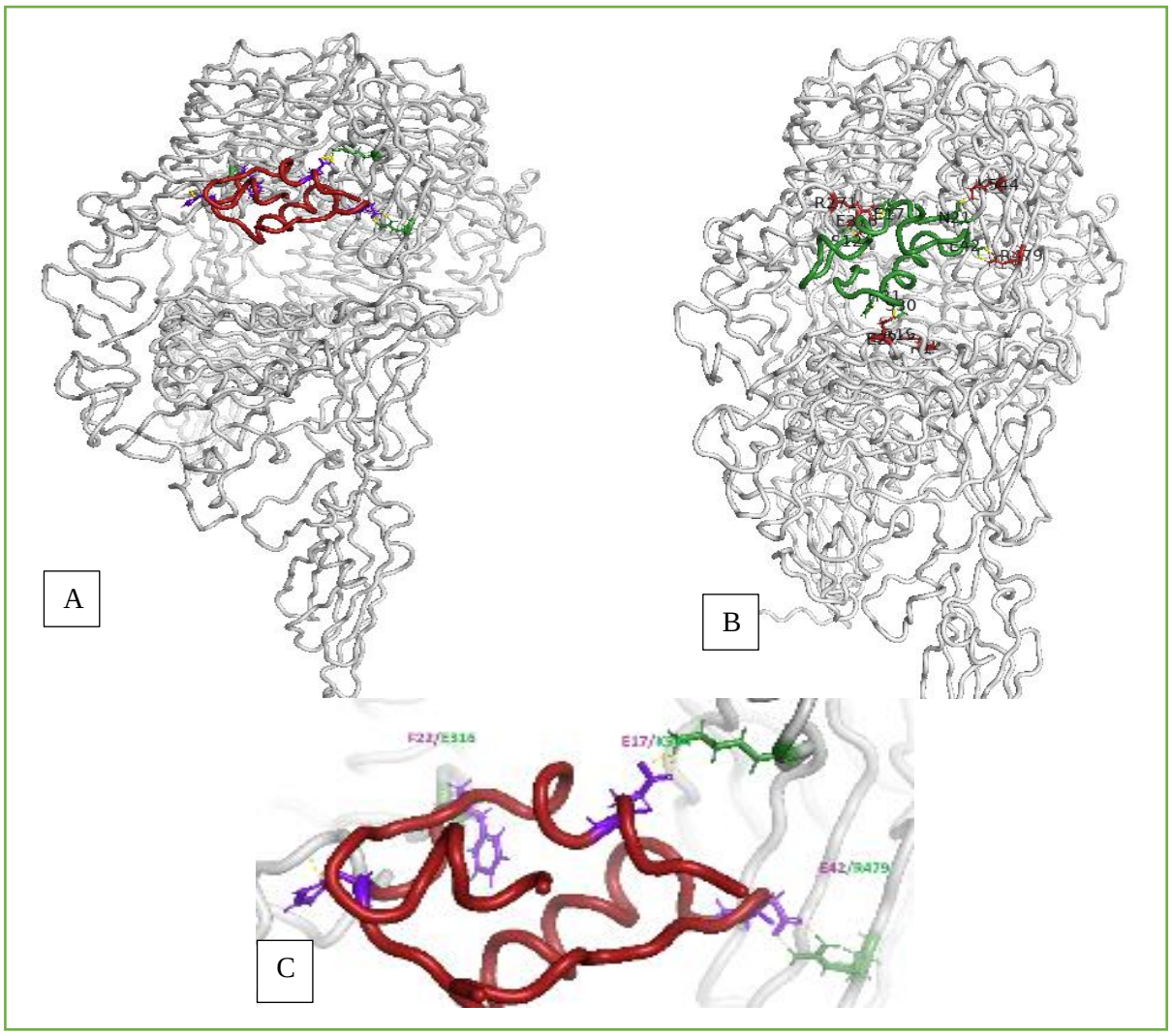

Figure11: insulin-ECD-IR interaction at 200ns. (A) side view of insulin-ECD-IR complex, location of insulin(red). (B)side-view of insulin interacting with ECD-IR at site2. (C) zoom-in insulin residues interacting with site2 residues.

Salt Bridges formation at ECD_IR apex

Studying the apex of the ectodomain of the insulin receptor at different simulation times and comparing them with the starting structure, we examined residual interactions, salt bridges, and hinge changes. At the apex of IR-ECD, residues Lys460, Asp464, and Asp574 form a network of switching salt bridges, ranging from inter-salt bridges to intra-salt bridges. We observe an inter-salt bridge formed between Lys460 and Lys460', while the latter residue forms an inter-salt bridge with Asp574. Meanwhile, Asp574' forms an inter-salt bridge with Lys460. This network of salt bridges switches with another network of salt bridges, such as Lys460' interacting with three residues simultaneously: Lys460 and Asp464. This latter salt bridge was observed at 200 ns of the simulation.

Before starting the simulation, the initial structure was examined for salt bridges or salt bridge networks, but none were observed at the apex of the ectodomain. Around 20 ns into the simulation,

interactions were formed between Lys460 and Asp574', while Lys460' formed interactions with Asp574 (Fig. 12). It is possible that each Lys460 can participate in either an inter- or intra-subunit salt bridge, and in a globally asymmetric conformation, these two lysines cannot both participate in the same type of bridge; when one is intra-subunit, the other is inter-subunit. This switching network is maintained throughout the 200 ns simulation.

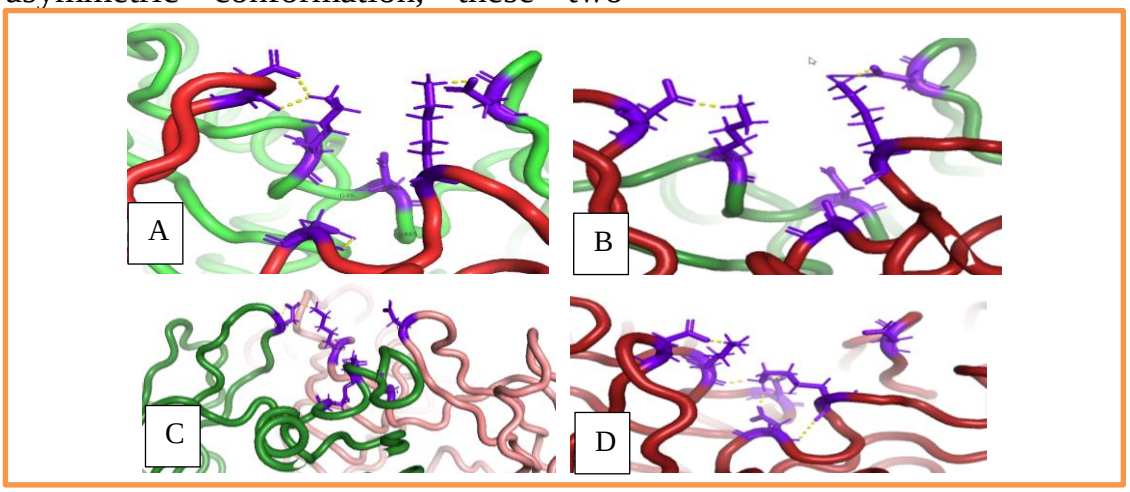

Figure (12) Location of the salt bridges at the apex ECD-IR**:** at the apex of the dimer intra-subunit Lys460-Arg464; and intersubunit Lys460-Arg574. A) at 9ns no salt bridge network. B) at 20ns no salt bridge network (C) at 60 ns salt bridge network is formed D) at 200 ns of simulation time the salt bridge network is maintained

Salt Bridges depletion at the L1/FnIII-2 subdomains interface

Interdomain interactions often involve salt bridges, and the insulin receptor (IR) in its inactive state exhibits a different salt bridge pattern compared to its active states. In our study, we observed changes in several important interdomain salt bridge interactions (Fig. 13, 14). The Glu154-Arg81 salt bridge, observed in the crystal structure, remained intact during the initial 20 ns of simulation on both interfaces of L1/FnIII-2. However, once an interaction between insulin and IR site 2 occurred, the Glu154-Arg81 salt bridge at the interface near the site of insulin interaction (L1/FnIII-2') broke down, while the equivalent residues remained intact on the alternate interface (L1'/FnIII-2) throughout the simulation (Fig. 14). The disruption of the Glu154-Arg81 salt bridge locally increased the distance between the two subdomains L1 and FnIII-2'. The initial distance between the backbone of these residues was 9.1 Å, which increased to 15 Å upon salt bridge breakage at 20 ns, and the gap between the two subdomains reached 18.2 Å (Fig. 14).

Several salt bridges exist within the L1-FnIII-2 interface besides Glu154-Arg81. Another salt bridge present in the inactive state of IR between L1-FnIII-2' (L1'-FnIII-2) is Lys102-Glu70. However, as the interaction between insulin and IR begins at 20 ns of simulation time, the bond between Lys102 and Glu70 (Fig. 15A) breaks on the side of the receptor closer to IR-site 2 interacting with insulin,

while the Lys102-Glu70 salt bridge on the other side of the monomer remains intact (Fig. 15B). The interaction between insulin and the insulin receptor at site 2 not only disrupts the salt bridge but also leads to the separation of L1 and FnIII-2'. The initial distance between the backbones of Lys102 and Glu70 with the salt bridge intact was 5.1 Å, increasing to 29.8 Å at 20 ns of simulation time, maintaining this range throughout the 200 ns simulation.

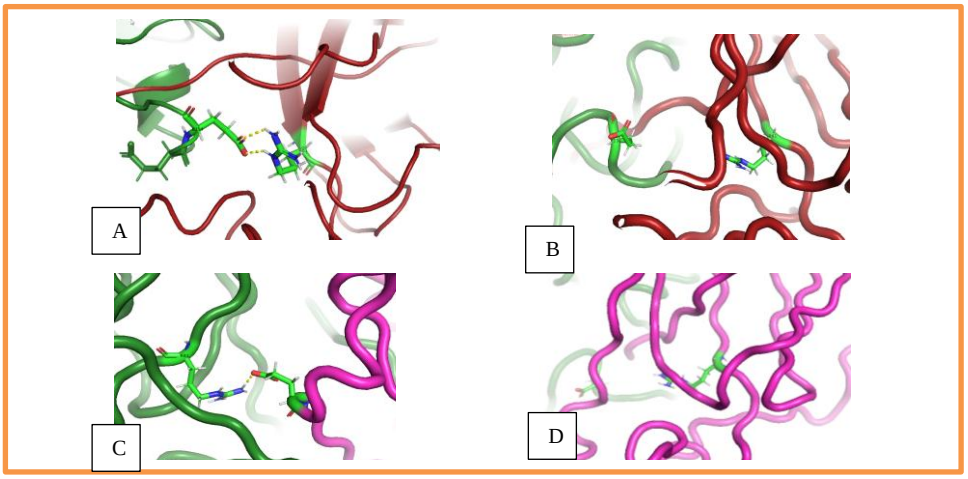

Figure13: Presence/absence of Glu^{154}-Arg^{81} salt bridge interactions across the L1/FnIII-2 interfaces, through different simulation time. A) Present at the crystal structure (starting structure). B) salt bridge breakage starts at the 20ns. C) at 135ns salt bridge is maintained intact on the alternate interface. D) Glu^{153}-Arg^{81} is broken at 135ns on interface close to insulin interaction with IR-site2

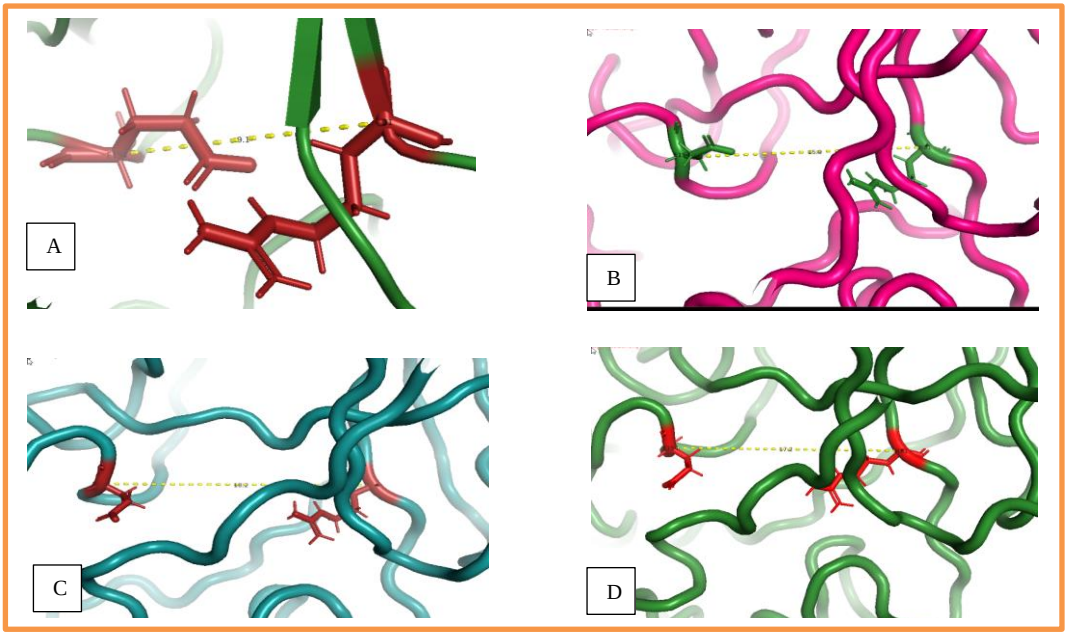

Figure 14: Salt bridge E154-R81(L1/FnIII-2') breakage (A)distance between L1 and FnIII-2' at the starting structure residues forming salt bridge is 9.1A (B) distance between the residues forming salt bridge at 20ns is 15A. (C) salt bridge breakage at 101, distance between L1 and FnIII-2'(E154 and R81) is 15A (D) salt bridge breakage between L1 and FnIII-2'(E154 and R81) at 200ns the distance is 15A

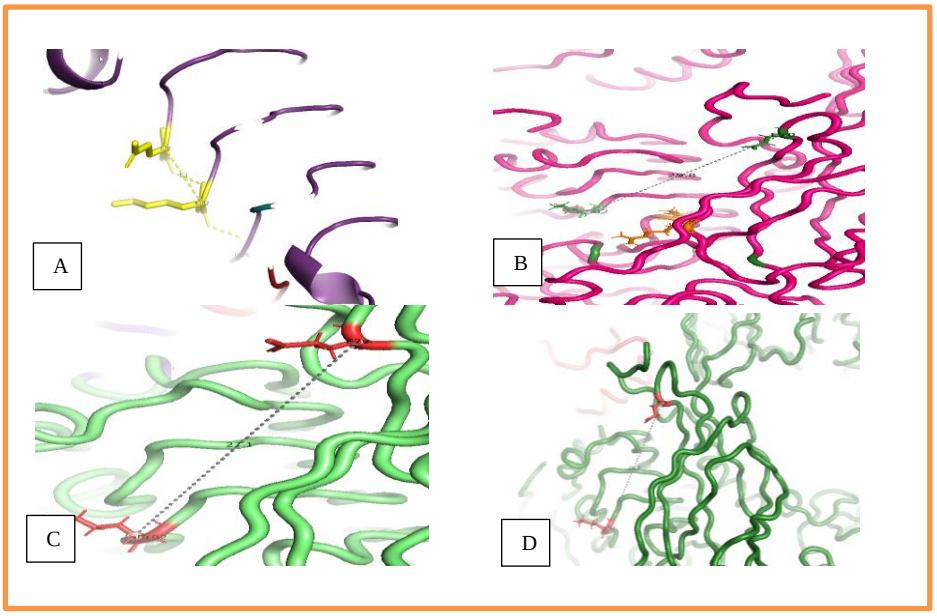

Figure 15: Presence/ absence of Salt bridge within L1-FnIII-2' between K102 and E70 respectively at different simulation time(A) Starting structure, salt bridge is present between L1 and FnIII-2' the distance within the salt bridge is 5.1A (B) salt bridge is broken, the distance at 20ns between K102 and E70 is 29.8A. (C) salt bridge between L1 and FnIII-2' (K102 and E70) at 101ns the distance between is 28.7A (D) salt bridge between L1 and FnIII-2' at 200ns the distance between K102 and E70 is 27.7A

DISCUSSION

In our study, we observed at the outset of the simulation that the initial recognition between insulin and the insulin receptor (IR) initiates through two simultaneous events. First, the insulin molecule reorients itself, directing its hexamer-forming surface towards the receptor surface. Concurrently, the insulin molecule displaces towards the insulin receptor, reaching its maximum reconfiguration around 60 ns into the simulation time (Fig. 6). Insulin monomers exist in two distinct allosteric forms known as "T-form" and "R-form" insulin, distinguished by the structure of the first eight residues of the N-terminal of the B-chain (F1-G8). The initial structure of insulin used in our simulations is in the T-state form (PDB: 1MSO). By 5 ns into the simulation, insulin undergoes a conformational change and temporarily adopts the R-state form (PDB: 1ZNI) [24], altering residues (F1-G8). In T-insulin, the N-terminal adopts an extended loop configuration, whereas in R-insulin, it forms a coiled loop. This observation supports experimental findings suggesting that the conformational change from T-form to R-form in insulin is not merely an artifact of crystallization [4]. We propose that R-insulin is an intermediate transient state that insulin temporarily adopts before returning to its T-insulin configuration. Notably, only T-insulin complexes have been observed with IR, suggesting a functional preference for the T-state. The rationale and benefits of this temporary conformational change remain unclear. Insulin undergoes a conformational change, particularly in the type-II β-turn between residues B20-B23, to prepare for interaction with IR site 1. Experimental studies indicate that insulin must reconfigure its C-terminal B-chain to

expose chain A and facilitate cross-linking between TyrB16 and PheB24 with the N-terminal region of the receptor α chain [25,26]. This reorientation of the insulin B-chain's C-terminal segment is crucial for insulin-site 1 IR interaction [4]. We measured the dimensions of the β-turn to assess the insulin chain's mobilization capability in preparation for site 1 interaction, initially noting a slight progressive increase in distance from 9.8 Å between TyrB16 and PheB24 to 10.8 Å. However, no further increase in dimension was observed beyond this point.

In our study, significant conformational alterations akin to those observed during insulin-site 1 binding were absent. Instead, insulin molecules reoriented and migrated towards the insulin receptor surface, positioning themselves similarly to when binding to site 2. Comparing the starting structure of insulin to simulated structures at different time points (Fig. 4, 5), no substantial conformational changes were observed within insulin molecules, except for the transient change from T-form to R-form and back to T-form. The primary modifications involved the reorientation and migration of insulin towards the receptor, aligning the hexamer-binding surface of insulin with the insulin binding site 2. To gain deeper insights into insulin's initial behavior towards its receptor, we analyzed intermolecular hydrogen bond interactions. Specifically, we studied the number and duration of hydrogen bonds between insulin and IR throughout the simulation [27].

This study utilized various tools such as PyMOL and the `gmx hbond` module from GROMACS to analyze hydrogen bond formations. Molecular dynamics simulations were conducted to investigate the dynamic behavior and differences in protein dynamics between insulin and the insulin receptor (IR) during their initial association. The main chain root mean square deviations (RMSD) were calculated for the trajectories of insulin and the insulin receptor, using the backbone after least square fitting to C-alpha atoms with the ‘‘g_rms’’ tool. Over the 230 ns simulation period, the insulin receptor maintained a nearly constant conformation, with a maximum backbone RMSD value of approximately 1 nm (Fig. 5A). In contrast, insulin exhibited higher deviations, reaching a maximum RMSD of 1.5 nm. The initial peak in insulin RMSD occurred within the first 60 ns, followed by another significant deviation around 200 ns (Fig. 5B). Both insulin and the insulin receptor showed stable RMSD values for the remainder of the simulation period. These RMSD profiles suggest that insulin experienced more dynamic fluctuations compared to the relatively stable insulin receptor, indicating potential conformational changes or flexibility in insulin that require further investigation.

The dynamic behavior of residues was further analyzed using root mean square fluctuations (RMSF) for insulin and the insulin receptor. RMSF values for insulin receptor residues ranged from 0.5 to 8 nm over the entire simulation, with most residues fluctuating between 0.5 to 4 nm. Residues in the FnIII-1 region, particularly at the αCT subdomain close to site 1 of insulin interaction, exhibited the highest flexibility, reaching up to 8 nm (Fig. 5A). In contrast, insulin residues showed RMSF values ranging from 0.5 to 2 nm, indicating overall lower fluctuation compared to the insulin receptor (Fig.

5B). Regions such as chain A C-terminal and chain B C-terminal exhibited larger fluctuations, suggesting potential involvement in dynamic interactions, possibly involving hydrogen bonds, that contribute to their stability. Radius of gyration (Rg) was employed to assess the compactness of insulin and the insulin receptor structures throughout the 200 ns simulation at 300 K. Rg, defined as the mass-weighted root mean square distance of atoms from their center of mass, provides insights into the overall dimensions of proteins. The Rg plot for insulin receptor demonstrated a consistent value throughout the simulation, indicating structural stability over time. In contrast, insulin initially showed an increased Rg value until approximately 60 ns, after which the system (insulin and insulin receptor) equilibrated and maintained stability for the remainder of the simulation (Fig. 7). These findings from RMSD and Rg analyses underscore that the insulin receptor maintained structural steadiness, while insulin exhibited relatively higher dynamics and potential conformational flexibility.

Molecular recognition is the process in which biological macromolecules interact with each other through noncovalent interactions to form a specific complex. [29] In this study, the major result of MD simulations is the formation of insulin-IR-ECD complex. The process of complex formation is studied through the dynamic behavior of insulin and insulin receptor, which is governed by the specificity and affinity towards the binding partner. In all of the simulations insulin behaves and takes similar route in its interaction with insulin receptor, such as adopting the intermediate configuration of R-state at the beginning of the simulation to go back to T-state before any direct association with the receptor. In our study, except for a non-persistent interaction at the 9ns where $Asn^{A}18$ forms an intermittent hydrogen bonding with site2 residue Lys544, no interaction was observed between insulin and IR till the 15 ns of the simulation time. Our simulations suggest that two main changes take place along the pathway leading to the interaction of insulin to site2, the first change is the reorientation of insulin without significant conformational change within the molecule itself, the adaptation of new orientation leads to bringing the hexamerizing surface of insulin in closer contact with IR surface. Insulin reorientation is simultaneously taking place with its movement towards the receptor surface, this will probably lead to the dehydration of both the ligand and the extracellular surface of IR, bringing the ligand at close proximity to the β-sheet of site2 IR [Fig.7].

At the 15 ns insulin shows its first association with IR. Insulin's dynamical behavior towards insulin receptor leads to the formation of the first interaction through a single hydrogen bond between $E^{A}17$, an insulin residue at chain A, with K544 an IR residue located at FnIII-1 site2 (Fig.8). This fast interaction agrees with experimental measurements which have demonstrated that ligand–IR interaction at site2 is a rapid weak interaction with low affinity when compared to site1 interaction. [12,30,31] We expect that the reason behind the relatively speedy interaction is because the ligand doesn't require conformational

changes to interact with site2, comparing it to what happens to insulin in its interaction at site1-IR where insulin conformational change is a prerequisite in the interaction. The other reason behind this fast-molecular recognition interaction is the location of site2 which is relatively more accessible than site 1 and doesn't require the binding to 3 different elements beside undergoing conformational changes. As simulation proceeds more residues from insulin will get involved with insulin receptor and stronger interactions with site2 are observed, as demonstrated in (Fig9) showing simulations at 15,20,60 and 112ns. Insulin receptor Site2 constitutes of the following residues located at FnIII-1: Y477, R479, K484 L486, R488, P537, L552, R554, while the hexamerizing-forming surface of insulin, constituting the following residues: $S^{A}12$, $L^{A}13$, $Y^{A}14$, $E^{A}17$, $Q^{B}4$, $H^{B}10$, $Q^{B}13$, $L^{B}17$, $V^{B}18$, $Q^{B}21$. [4, 12, 23]

The process of insulin-insulin receptor molecular recognition is noted on the first association between site2 of IR and the hexamerizing insulin surface through hydrogen bond formation. Hydrogen bonding is considered as a key interaction determining the protein-ligand binding affinity. The predominant interactions observed in our study are between side-chains of $Glu^{A}17$ (insulin) interacting with R479, R488 or K544 of FnIII-1(IR) through two hydrogen bonds, while $Glu^{B}42$(insulin) interacts with Arg479, of FnIII-1 of the same monomer using another two hydrogen bonds. The interacted glutamic acid is a polar, negatively charged hydrophilic amino acid that interacts with another polar, positively charged arginine and lysine amino acid residues of insulin receptor. Insulin residue $F^{B}22$(insulin) is also observed to interact with Glu316 of L2 subdomain of the alternate monomer with a single hydrogen bond, but the latter interaction is intermittent and often breaks during the simulation, experimental measurements have demonstrated that ligand–IR interaction at site2 is a rapid weak interaction with low affinity.

At 101ns of simulation, insulin gets more involved with IR, beside maintaining the interaction with FnIII-1, interactions spread to involve subdomains L1 and CR, as hydrogen bonding is formed between $S^{A}12$ with E316, $S^{B}30$ with E22, $H^{B}31$ with R19 (Fig. 10A) At 125 ns of simulation, more insulin and IR interactions at L1, CR subdomains: $S^{A}12$ interacts with E316 using 3HB and interacting with R791 with 2HB, Q5 with N268, I10 with C274, S9 with K265(Fig.10B), but as simulation continues, insulin starts to lose interactions with ECD-IR, at 135 ns of simulation, interactions are decreasing: S30, H31, E34, Y36 interact with IR, while At the 200 ns interactions are with: Q5, S30, reduction of interaction continues even after230 ns: S11, S30, H31. At 230 ns: S30, H31. After the first interaction between insulin and IR, we continue to study the dynamics of the insulin_ECD_IR relationship using molecular dynamic simulation. Lys460, Asp464, and Asp574 residues create an apparent asymmetric switching network at the apex of the ectodomain. There was no salt bridge formation within this switching network prior to the first 20 ns of simulation, which is consistent with insulin and site 2 of IR not interacting at all. Starting the 20ns of simulation an intra-subunit Lys460-Asp464 salt bridge

that ruptures intermittently but remains mostly stable was observed (Fig.12) while there is no Lys460'-Asp464' salt bridge. Another salt bridge is observed between Lys460'and Asp574, whereas no Lys460-Asp574'bridge is seen, because Lys460 is occupied at the same time in the Lys460-Asp464 intra-subunit salt bridge. It is possible that each Lys460 can participate in either an inter- or intra-subunit salt bridging, and that in a globally asymmetric conformation, these two lysines cannot both participate in the same type of bridge; when one is intra-subunit, the other is inter-subunit. This switching network is maintained through the 200ns simulation. It has been suggested that the salt bridge network when it is in an intersubunit state helps to tighten and lock the two monomers interfaces together, whereas the intrasubunit salt bridge network frustrates the closing of the L2/F1 interface. [36] This behavior plays a crucial role in the negative cooperativity, a feature which characterizes insulin receptor in its active state. [32-35]

Interdomain interactions often involve salt-bridge interactions between residues, which play a role in receptor stability or as in insulin receptor salt-bridge aid in imposing the auto-inhibitory inactive state of IR. L1/FnIII-2 salt-bridges interfaces were predicted based on the IR-ECD structure.[4,36] The Glu154-Arg81 salt bridge observed at the crystal structure and maintained an intact bonding throughout the first 20ns of simulation on both interfaces of L1/FnIII-2, however once an interaction between insulin and IR site2 takes place, the Glu154-Arg81 salt bridge at the interface close to the site of insulin interaction (L1/FnIII-2') breaks down, while the equivalent residues remains intact on the opposite interface of (L1'/FnIII-2) throughout the simulation. (Fig.13) The breakage of Glu154-Arg81 salt bridge will locally increase the distance between the two subdomains L1 and FnIII-2', the distance between the two residues' backbone at the starting structure is 9.1Å, upon salt-bridge breakage at the 20ns of the simulated structures, the distance will reach 15Å between the same residues Glu154 and Arg81. (Fig.14) Several salt bridges exist within the interface between L1 and FnIII-2 beside the Glu154-Arg81, another salt bridge that exists in IR inactive state between L1-FnIII-2'(L1'-FnIII-2) is Lys102-Glu70, but as the interaction between insulin and IR starts at the 20ns of simulation time, the bond between Lys102 and Glu70(Fig.14A) breaks on one side of the receptor which is closer to IR-site2 interacting with insulin, meanwhile the Lys102-Glu70 salt bridge on the other side of the monomer remains intact. (Fig15B) Insulin -insulin receptor interaction at site 2 doesn't only cause the disruption of the salt bridge but it will lead to the separation of L1 and FnIII-2'. The distance between the backbone of Lys102 and Glu70 at the starting structure with the salt bridge intact between the two residues is 5.1Å, at 20ns of the simulation time the distance increases to 29.8Å and remains in this range throughout the simulation of 200ns.

CONCLUSION

In our molecular dynamics simulation study of insulin-IR binding, we observed the initial interaction between insulin and the insulin receptor binding site, adopting a crystallographically validated binding pose. Our unbiased atomistic MD simulations consistently identified and

maintained this first binding site, occurring between the hexamer-forming surface of insulin and binding site 2, specifically the outward-facing β-sheet surface of the FnIII-1 domain. Importantly, this pose was achieved without user intervention or prior knowledge of the binding site. Moreover, our simulations elucidated the binding pathway that facilitates subsequent interactions between insulin and binding site 1 of the IR. We observed the formation of salt bridges at the apex of the IR ectodomain upon insulin-site 2 interaction. These populated salt bridges play a critical role in insulin-site 1 interactions by regulating the number of insulin molecules bound to site 1, a phenomenon known as negative cooperativity in the insulin receptor. Insulin-binding sites 1(1') are partially occluded due to domain L1 engaging with domain FnIII-2' and domain L1' engaging with domain FnIII-2. Interaction of insulin via its hexamer-forming surface with binding site 2 leads to changes in salt bridges formed by amino acid residues between subdomains L1 and FnIII-2'. Our simulations demonstrated the disruption of bonds between amino acid residues K102 with E793, E124 with E755, and E154 with R804 in L1 and FnIII-2', respectively. Dissociation from these interactions allows elements of L1 and aCT' of binding site 1 to rearrange freely and enhance their affinity for insulin molecules. This release from an autoinhibitory conformation, partially imposed by the interaction between L(L1')1 and FnIII-2', supports our hypothesis that site 2 receptor activation is crucial for facilitating higher affinity insulin-site 1 interactions.

Acknowledgments

The work presented here was conducted at the West Center for Computational Chemistry and Drug Design located at Saint Joseph University, Philadelphia. The authors would like to acknowledge the entire staff of the West Center for continuous help and technical support.

Declarations

Ethics approval and consent to participate
Not Applicable

Consent for publication

Not applicable

Availability of data and material

All data underlying the results are available as part of the article and no additional source data are required.

Funding

The Ministry of Higher Education and Scientific Research of Libya supported this work

Authors' contributions

M.P. oversight, resources and guidance **K.R.** conceived of the presented idea and guidance **D.S.** performed the work

Competing interests

M.P. oversight, resources and guidance K.R. conceived of the presented idea and guidance D.S. performed the work

REFERENCES

1. Federation ID. IDF diabetes atlas 8th edition. International diabetes federation. 2017:905-11.
2. Pollak M. The insulin receptor/insulin-

like growth factor receptor family as a therapeutic target in oncology. Clinical cancer research. 2012; 18(1):40-50. DOI:10.1158/1078-0432.CCR-11-0998

3. Nathan DM, Buse JB, Davidson MB, Ferrannini E, Holman RR, Sherwin R, Zinman B. Medical management of hyperglycemia in type 2 diabetes: a consensus algorithm for the initiation and adjustment of therapy: a consensus statement of the American Diabetes Association and the European Association for the Study of Diabetes. Diabetes care. 2009; 32(1):193-203. DOI: 10.2337/dc08-9025

4. Lawrence MC. Understanding insulin and its receptor from their three-dimensional structures. Molecular metabolism. 2021; 52:101255. DOI: 10.1016/j.molmet.2021.101255

5. Croll TI, Smith BJ, Margetts MB, Whittaker J, Weiss MA, Ward CW, Lawrence MC. Higher-resolution structure of the human insulin receptor ectodomain: multi-modal inclusion of the insert domain. Structure. 2016; 24(3):469-76.

6. Smith GD, Pangborn WA, Blessing RH. The structure of T6 human insulin at 1.0 Å resolution. Acta Crystallographica Section D: Biological Crystallography. 2003; 59(3):474-82. DOI: 10.1107/S0907444902023685

7. Lawrence MC. Understanding insulin and its receptor from their three-dimensional structures. Molecular metabolism. 2021; 52:101255. DOI: 10.1016/j.molmet.2021.101255

8. White MF, Kahn CR. Insulin action at a molecular level–100 years of progress. Molecular metabolism. 2021;52:101304. DOI:10.1016/j.molmet.2021.101304

9. Gutmann T, Kim KH, Grzybek M, Walz T, Coskun Ü. Visualization of ligand-induced transmembrane signaling in the full-length human insulin receptor. Journal of Cell Biology. 2018; 217(5):1643-9. DOI: 10.1083/jcb.201711047

10. Maruyama IN. Mechanisms of activation of receptor tyrosine kinases: monomers or dimers. Cells. 2014; 3(2):304-30. DOI: 10.3390/cells3020304

11. Scapin G, Dandey VP, Zhang Z, Prosise W, Hruza A, Kelly T, Mayhood T, Strickland C, Potter CS, Carragher B. Structure of the insulin receptor–insulin complex by single-particle cryo-EM analysis. Nature. 2018; 556 (7699):122-5. DOI: 10.1038/nature26153

12. Uchikawa E, Choi E, Shang G, Yu H, Bai XC. Activation mechanism of the insulin receptor revealed by cryo-EM structure of the fully liganded receptor–ligand complex. Elife. 2019; 8:e48630. DOI: 10.7554/eLife.48630

13. Xu Y, Margetts MB, Venugopal H, Menting JG, Kirk NS, Croll TI, Delaine C, Forbes BE, Lawrence MC. How insulin-like growth factor I binds to a hybrid insulin receptor type 1 insulin-like growth factor receptor. Structure. 2022; 30(8):1098-108. DOI:10.1016/j.str.2022.05.007

14. Nielsen J, Brandt J, Boesen T, Hummelshøj T, Slaaby R, Schluckebier G, Nissen P. Structural investigations of full-length insulin receptor dynamics and signalling. Journal of molecular biology. 2022; 434(5):167458.
DOI: 10.1016/j.jmb.2022.167458

15. Batishchev OV, Kuzmina NV, Mozhaev AA, Goryashchenko AS, Mileshina ED, Orsa AN, Bocharov EV, Deyev IE, Petrenko AG. Activity-dependent conformational transitions of the insulin receptor–related receptor. Journal of Biological Chemistry. 2021; 296:100534
DOI: 10.1016/j.jbc.2021.100534

16. Gutmann T, Schäfer IB, Poojari C, Brankatschk B, Vattulainen I, Strauss M, Coskun Ü. Cryo-EM structure of the complete and ligand-saturated insulin receptor ectodomain. Journal of Cell Biology. 2019; 219(1):e201907210. DOI: 10.1083/jcb.201907210

17. Massague J, Pilch PF, Czech MP. Electrophoretic resolution of three major insulin receptor structures with unique subunit stoichiometries. Proceedings of the National Academy of Sciences. 1980; 77(12):7137-41. DOI: 10.1073/pnas.77.12.7137

18. Sinha S, Tam B, Wang SM. Applications of molecular dynamics simulation in protein study. Membranes. 2022; 12(9):844. DOI: 10.3390/membranes12090844

19. Mohammadiarani H, Vashisth H. All-atom structural models of the transmembrane domains of insulin and type 1 insulin-like growth factor receptors. Frontiers in Endocrinology.

2016; 7:68. DOI: 10.3389/fendo.2016.00068
20. De Meyts P, Roth J, Neville Jr DM, Gavin III JR, Lesniak MA. Insulin interactions with its receptors: experimental evidence for negative cooperativity. Biochemical and biophysical research communications. 1973; 55(1):154-61. DOI: 10.1016/S0006-291X(73)80072-5
21. McKern NM, Lawrence MC, Streltsov VA, Lou MZ, Adams TE, Lovrecz GO, Elleman TC, Richards KM, Bentley JD, Pilling PA, Hoyne PA. Structure of the insulin receptor ectodomain reveals a folded-over conformation. Nature. 2006; 443(7108):218-21.
22. Astuti AD, Refianti R, Mutiara AB. Molecular dynamics simulation on protein using GROMACS. Int J Comput Sci Inf Security. 2011; 9:16-20.
23. Gorai B, Vashisth H. Progress in simulation studies of insulin structure and function. Frontiers in endocrinology. 2022; 13:908724. DOI: 10.3389/fendo.2022.908724
24. Bentley G, Dodson E, Dodson GU, Hodgkin D, Mercola DA. Structure of insulin in 4-zinc insulin. Nature. 1976; 261(5556):166-8. DOI: 10.1038/261166a0
25. Huang K, Xu B, Hu SQ, Chu YC, Hua QX, Qu Y, Li B, Wang S, Wang RY, Nakagawa SH, Theede AM. How insulin binds: The B-chain α-helix contacts the L1 β-helix of the insulin receptor. Journal of molecular biology. 2004; 341(2):529-50. DOI: 10.1016/j.jmb.2004.05.023
26. Xu B, Hu SQ, Chu YC, Huang K, Nakagawa SH, Whittaker J, Katsoyannis PG, Weiss MA. Diabetes-associated mutations in insulin: consecutive residues in the B chain contact distinct domains of the insulin receptor. Biochemistry. 2004; 43(26):8356-72. DOI: 10.1021/bi0497796
27. Hao MH. Theoretical calculation of hydrogen-bonding strength for drug molecules. Journal of chemical theory and computation. 2006; 2(3):863-72. DOI: 10.1021/ct0600262
28. Baig MH, Sudhakar DR, Kalaiarasan P, Subbarao N, Wadhawa G, Lohani M, Khan MK, Khan AU. Insight into the effect of inhibitor resistant S130G mutant on physico-chemical properties of SHV type beta-lactamase: A molecular dynamics study. PLoS One. 2014; 9(12):e112456. DOI: 10.1371/journal.pone.0112456
29. Du X, Li Y, Xia YL, Ai SM, Liang J, Sang P, Ji XL, Liu SQ. Insights into protein–ligand interactions: mechanisms, models, and methods. International journal of molecular sciences. 2016;17(2):144. DOI: 10.3390/ijms17020144
30. Subramanian K, Fee CJ, Fredericks R, Stubbs RS, Hayes MT. Insulin receptor-insulin interaction kinetics using multiplex surface plasmon resonance. Journal of Molecular Recognition. 2013 ;26(12):643-52. DOI: 10.1002/jmr.2307
31. Whittaker L, Hao C, Fu W, Whittaker J. High-affinity insulin binding: insulin interacts with two receptor ligand binding sites. Biochemistry. 2008 ;47(48):12900-9. DOI: 10.1021/bi801693h
32. De Meyts P. The structural basis of insulin and insulin-like growth factor-I receptor binding and negative co-operativity, and its relevance to mitogenic versus metabolic signalling. Diabetologia. 1994 ;37(Suppl 2):S135-48. DOI: 10.1007/BF00400837
33. Meyts PD, Van Obberghen E, Roth J, Wollmer A, Brandenburg D. Mapping of the residues responsible for the negative cooperativity of the receptor-binding region of insulin. Nature. 1978; 273(5663):504-9. DOI: 10.1038/273504a0
34. De Meyts P, Roth J, Neville Jr DM, Gavin III JR, Lesniak MA. Insulin interactions with its receptors: experimental evidence for negative cooperativity. Biochemical and biophysical research communications. 1973 ;55(1):154-61. DOI: 10.1016/S0006-291X(73)80072-5
35. Sun WX, Zhang KH, Zhou Q, Hu SH, Lin Y, Xu W, Zhao SM, Yuan YY. Tryptophanylation of insulin receptor by WARS attenuates insulin signaling. Cellular and Molecular Life Sciences. 2024; 81(1):25. DOI: 10.1007/s00018-023-05082-2
36. Sena MM, Gromiha MM, Chatterji M, Khedkar A, Ranganathan A. Mapping Structural Drivers of Insulin and its Analogs at the IGF-1 Receptor Using Molecular Dynamics and Free Energy Calculations. bioRxiv. 2023 :2023-12.
37. Talbot K, Wang HY, Kazi H, Han LY, Bakshi KP, Stucky A, Fuino RL, Kawaguchi KR, Samoyedny AJ, Wilson RS, Arvanitakis Z.

Demonstrated brain insulin resistance in Alzheimer's disease patients is associated with IGF-1 resistance, IRS-1 dysregulation, and cognitive decline. The Journal of clinical investigation. 2012; 122(4):1316-38. DOI: 10.1172/JCI59903

38. Samson SL, Vellanki P, Blonde L, Christofides EA, Galindo RJ, Hirsch IB, Isaacs SD, Izuora KE, Wang CC, Twining CL, Umpierrez GE. American Association of Clinical Endocrinology Consensus Statement: comprehensive type 2 diabetes management algorithm–2023 update. Endocrine Practice. 2023; 29(5):305-40. DOI: 10.2337/dc08-9025

39. Alyas J, Rafiq A, Amir H, Khan SU, Sultana T, Ali A, Hameed A, Ahmad I, Kazmi A, Sajid T, Ahmad A. Human insulin: history, recent advances, and expression systems for mass production. Biomedical Research and Therapy. 2021; 8(9):4540-61. DOI 10.15419/bmrat.v8i9.692.

40. Dhayalan B, Chatterjee D, Chen YS, Weiss MA. Structural lessons from the mutant proinsulin syndrome. Frontiers in Endocrinology. 2021; 12:754693. DOI: 10.3389/fendo.2021.754693

41. Liang Y, Chen Q, Zhou E, Bi J, Wang J, Li Y, Li L. Methyl ferulic acid ameliorates prolonged high insulin-induced insulin release and synthesis in pancreatic β-cells via the miR-378b–PI3K–AKT pathway. Journal of Functional Foods. 2023; 105:105568. DOI: 10.1016/j.jff.2023.105568

42. Du Z, Su H, Wang W, Ye L, Wei H, Peng Z, Anishchenko I, Baker D, Yang J. The trRosetta server for fast and accurate protein structure prediction. Nature protocols. 2021; 16(12):5634-51. DOI: 10.1038/s41596-021-00628-9

43. Šali A, Blundell TL. Comparative protein modelling by satisfaction of spatial restraints. Journal of molecular biology. 1993; 234(3):779-815. DOI: 10.1006/jmbi.1993.1626

44. Pettersen EF, Goddard TD, Huang CC, Couch GS, Greenblatt DM, Meng EC, Ferrin TE. UCSF Chimera—a visualization system for exploratory research and analysis. Journal of computational chemistry. 2004; 25(13):1605-12. DOI: 10.1002/jcc.20084

How to cite this article:
Diaf SR; Khashan R; Moore P. Computational Method of Molecular Dynamics Simulation Identifies Insulin Receptor Binding Site 2 as the Primary Site for Insulin Binding. Med. Pharm. J. 2024; 3(4): 137-159.
DOI: 10.55940/medphar202488
Available from: http://pharmacoj.com/ojs/index.php/Medph/article/view/88